Interaction of cavitation bubbles on a wall

Nicolas Bremond,[a] Manish Arora, Stephan M. Dammer, and Detlef Lohse
Physics of Fluids, Department of Applied Physics, University of Twente, 7500 AE Enschede, The Netherlands

(Received 27 April 2006; accepted 15 August 2006; published online 8 December 2006)

We report experimental and numerical investigations on the dynamics of the cavitation of bubbles on a solid surface and the interaction between them with the help of controlled cavitation nuclei: hemispherical bubbles are nucleated from hydrophobic microcavities that act as gas traps when the substrate is immersed in water. The expansion of these nuclei is triggered by an impulsive lowering of the liquid pressure. The patterning of the substrate allows us to control the number of bubbles and the distance between them. Each hemispherical bubble experiences the effect of its mirror image. Correspondingly, an isolated hemispherical bubble together with its mirror image behaves like a free spherical bubble, i.e., its dynamics is well described by the Rayleigh-Plesset equation. We employ the setup to study the dynamics of two and more bubbles in a row at controlled and fixed distances from each other. For weak interaction, namely when the maximum size of the bubbles is smaller than the bubble distance, the dynamics of the system is well captured by an extended Rayleigh-Plesset equation, where mutual pressure coupling through sound emission is included. Bubble pairs last longer than an isolated bubble as neighboring bubbles modify the surrounding pressure and screen each other. For strong interaction, obtained by increasing the tensile stress or decreasing the bubble distance, the bubbles eventually flatten and form a liquid film between each other which can rupture, leading to coalescence. The film thinning is inertia dominated. A potential flow boundary integral simulation captures the overall shape evolution of the bubbles, including the formation of jets horizontal to the wall. These horizontal jets are caused by symmetry breaking due to the neighboring bubbles. © *2006 American Institute of Physics*. [DOI: 10.1063/1.2396922]

I. INTRODUCTION

Liquids rupture and form vapor bubbles when the liquid pressure is decreased beyond a critical tension. This phenomenon is known as cavitation.[1,2] *Homogeneous* nucleation refers to the cavitation of a pure liquid taking place from microscopic voids due to thermal fluctuations.[3] This type of nucleation has been observed to be initiated at a negative pressure of −140 MPa for ultrapure water at 42 °C (Ref. 4). In contrast, *heterogeneous* nucleation originates from the presence of submicroscopic air pockets at the solid/liquid interface on the wall of the container or on particles present in the liquid.[5] When the pressure is sufficiently reduced, these air pockets expand and bubbles emerge. The contamination of liquids in natural or industrial situations therefore weakens the ability of liquids to sustain high tension. For the same reason, cavitation is a very erratic process, notoriously difficult to control.

In this paper we demonstrate how we have succeeded to *control* the cavitation by predetermining nucleation sites on a hydrophobic solid wall immersed in water. In this way we can quantitatively and reproducibly study surface cavitation. Preliminary results on uncontrolled and controlled surface cavitation have been reported in Bremond *et al.*[6] The mutual interaction of bubbles in a two-dimensional bubble cluster is studied in Ref. 7. Here, we focus on the bubble-bubble interaction, bubble coalescence, and the comparison between experiments and boundary integral simulations.

Lord Rayleigh[8] was the first to analyze the dynamics of the collapse of a single and spherical cavity in a surrounding liquid. This pioneering work on cavitation has been followed by many experimental and theoretical studies starting from the 1950s (see Ref. 9, the 1977 review of Plesset and Prosperetti), which led to a good understanding of the radial dynamics of an isolated bubble.[5,10] The interest on cavitation rose mainly by the need to better understand damages induced by such event.[11–13] The focusing power of collapsing bubbles can also be used for surfaces cleaning (see, e.g., Krefting *et al.*[14]). The knowledge on bubble dynamics got further boosted by the discovery and the explanation of single-bubble sonoluminescence,[15] a light-emitting bubble trapped in an oscillating acoustic field. However, in general, cavitation bubbles in an acoustic field will mutually interact, often in an uncontrolled way. This collective behavior has been addressed theoretically[16–18] and numerically.[19–22] A few experiments have been done on the interaction of bubbles using laser-induced cavitation[23,24] or focusing on the collapse of preexisting bubbles in gelatine,[25] or in salt crystals.[26] The main difficulty occurring in the experiments has been the coupling between radial and translational dynamics of the bubbles.

We have therefore designed an experimental procedure for controlling the locations of nucleation by keeping them fixed. The nucleation takes place from hydrophobic microcavities etched on a solid surface (Sec. II). These cavities act

[a]Present address: Laboratoire Colloïdes et Matériaux Divisés, ESPCI, 10 rue Vauquelin, 75231 Paris, France.

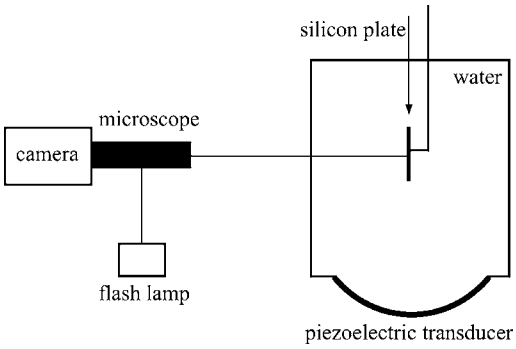

FIG. 1. Experimental setup.

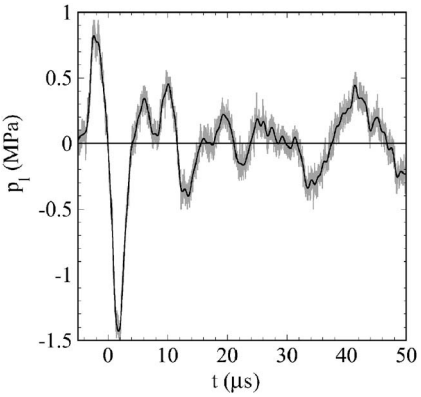

FIG. 2. Pressure signal averaged over 50 events recorded with an optic fiber (in gray) and the corresponding low-pass filtered signal (in black).

as gas traps once the substrate is immersed into water and they promote liquid fracture when the pressure is reduced. The dynamics of an isolated bubble for different forcing and geometry of the cavity is first described (Sec. III) and compared to the dynamics of a spherical bubble given by the Rayleigh-Plesset equation. The interaction of bubble pairs is investigated for weak coupling where the bubbles basically stay spherical (Sec. IV), and then for strong coupling for which they flatten and a thin film is formed between them which can rupture, leading to coalescence (Sec. V). In the strong-coupling regime obviously the Rayleigh-Plesset approach does not hold any longer due to the loss of spherical symmetry. This regime, however, can be studied with the help of potential flow boundary integral simulations (Sec. VI).

II. EXPERIMENTAL PROCEDURES

The experimental setup is depicted in Fig. 1. A piezoelectric transducer (Piezoson 100, Richard Wolf GmbH) is used as a pressure pulse generator. The device is made of two layers of piezoelectric components arranged on a portion of a sphere. It is connected to a rectangular tank containing 1 liter of Milli-Q water saturated with gas at room temperature ($\sim$20 °C). The transducer is driven by a high-voltage discharge and generates an acoustic wave whose features evolve as it propagates inside the tank. The liquid pressure p_l is characterized with the help of a fiber optic pressure hydrophone (FOPH 500, RP. Acoustics). The pressure is derived by measuring the reflected intensity of the laser beam at the fiber tip, which depends on the local impedance of the water changing as the pressure evolves.[27] An average over 50 recordings is reported in Fig. 2. The pressure wave is characterized by a high-pressure front followed by a negative pressure pulse lasting (in the case of Fig. 2) 4 μs and going down to around −1.4 MPa. A low-pass filter is then applied to the average signal in order to remove the high-frequency noise. The filtering avoids numerical errors when the dynamics of the bubbles is computed by using the experimental pressure recording as will be discussed in the next sections. The filtered pressure signal is also shown in Fig. 2.

The substrates are 3 mm $\times$5 mm plates diced from a silicon wafer. Cylindrical cavities 15 μm deep with a diameter D varying from 4 to 20 μm are etched on the wafer using the deep reactive ion etching (DRIE) technique. The substrate is finally made hydrophobic by coating the surface with perfluorodecyltrichlorosilane (FDTS) through vapor deposition. The advancing contact angle of water on such a surface is 106° ± 1°. With this procedure, we are able to control the spatial location of hydrophobic cavities which act as gas traps and therefore promote the nucleation of bubbles once the liquid pressure is lowered. As previously reported,[6] the number of successive nucleation events from a cavity depends on its size: the smaller the cavity diameter the larger the number of low-pressure pulses (shots) needed for removing all the entrapped air. The substrate is therefore pulled out of the water between each shot in order to evaporate the water contained in the cavity and so reactivate the artificial nucleation site.

The silicon plates are fixed on a thin rod, which is coupled to a three-axis translation stage (Linos Photonics, x.act LT100 ST). The substrates are then adjusted along the axis of the pressure transducer device and placed at different vertical locations in the water tank. Since the pressure wave shape evolves when the wave travels through the tank, different vertical positions correspond to different amplitudes p_m of the minimum pressure. The experiments have been conducted at three different vertical locations corresponding to a minimum pressure p_m equal to −1.4, −2.0, and −2.9 MPa. The cavitation event is recorded with a charged-coupled device (CCD) camera (FlowMaster, LaVision) through a long working distance microscope (Model K2, Infinity). The lighting is provided by a flash lamp in reflection mode (Fig. 1). The couple flash/camera is controlled via a programmable delay generator (BNC Model 555, Berkeley Nucleonics Corp.) in such a way that the diaphragm of the camera is closed 0.2 μs after the flash is switched on. This short exposure time minimizes motion blurring. Only one frame is taken during the overall process. The complete history of the bubble dynamics is scanned by tuning the time interval between the pressure pulse generator and the couple flash/camera. We stress here that each data point and each snapshot reported in this paper corresponds to one individual experiment. The standard deviation of the bubble size for several runs at the same observation time is less than 10%. The remarkable reproducibility of the observed phenomenon

allows this procedure; we can even produce movies of the cavitation event in this way (1 μs between successive frames).

III. THE ISOLATED BUBBLE

The time evolution of a spherical bubble is described by the Rayleigh-Plesset equation,[8,9,28]

$$R\ddot{R} + \frac{3}{2}\dot{R}^2 = \frac{1}{\rho}\left(p_i(t) - p_l(t) - \frac{2\sigma}{R} - \frac{4\mu}{R}\dot{R}\right). \quad (1)$$

Here, $R(t)$ is the bubble radius, ρ is the liquid density, σ is the surface tension, μ is the dynamic viscosity of the liquid, $p_l(t)$ is the pressure in the liquid far away from the surface, and $p_i(t)$ is the pressure inside the bubble, given by the sum of the gas pressure p_g, and the vapor pressure p_v. The gas inside the bubble is assumed to follow an isothermal compression. The assumption of isothermal behavior holds due to the small Peclet number $R\dot{R}/\kappa \ll 1$ (where κ is the thermal diffusivity) apart from the collapse when the spherical-bubble approximation breaks down anyhow. The artificial nuclei are found to be stable against gas diffusion in the liquid. Indeed, even if the negative pressure pulse is applied as long as 15 h after immersion of the probe, every single cavity still nucleates a bubble. According to Epstein and Plesset's analysis[29] of a bubble's lifetime in a liquid, this waiting time of 15 h gives a minimum radius of curvature of a few hundred microns. Making a rough analogy with the air pocket trapped inside the microcavity, the stretched liquid/gas interface on the cavities is therefore expected to be nearly flat, or at least the pressure jump across the interface is small compared to the atmospheric pressure p_0. If the bubble is at equilibrium at $t=0$, i.e., $p_i(0)=p_g(0)+p_v=p_0$, the pressure inside the bubble $p_i(t)$ is

$$p_i(t) = p_v + p_0\left(\frac{R_0}{R}\right)^3. \quad (2)$$

Here R_0 corresponds to the radius of half a sphere having the same volume of the cylindrical cavity etched in the substrate with a diameter D and a depth H, i.e., $R_0=(3HD^2/8)^{1/3}$.

One can estimate the initial velocity U_0 of the bubble wall by equating the kinetic energy of the flow to the work done by the pressure. Assuming that the far-field pressure is constant and equal to the amplitude p_m of the negative pressure pulse reported in Fig. 2, one obtains[9]

$$U_0 = \left(\frac{2}{3}\frac{p_v - p_m}{\rho}\right)^{1/2}. \quad (3)$$

According to the experimental pressure recordings, the initial velocity lies between 30 and 44 m/s. This rough estimate, Eq. (3), seems to well describe the data as shown in Fig. 3 for two forcing conditions and will be used later on for the two-bubble case.

We use an isolated bubble as a pressure probe by initially assuming that its dynamics obeys Eq. (1). We first interpolate the driving pressure $p_l(t)$ from the experimental pressure recording (Fig. 2) and then numerically integrate the Rayleigh-Plesset equation (1). The pressure amplitude is then

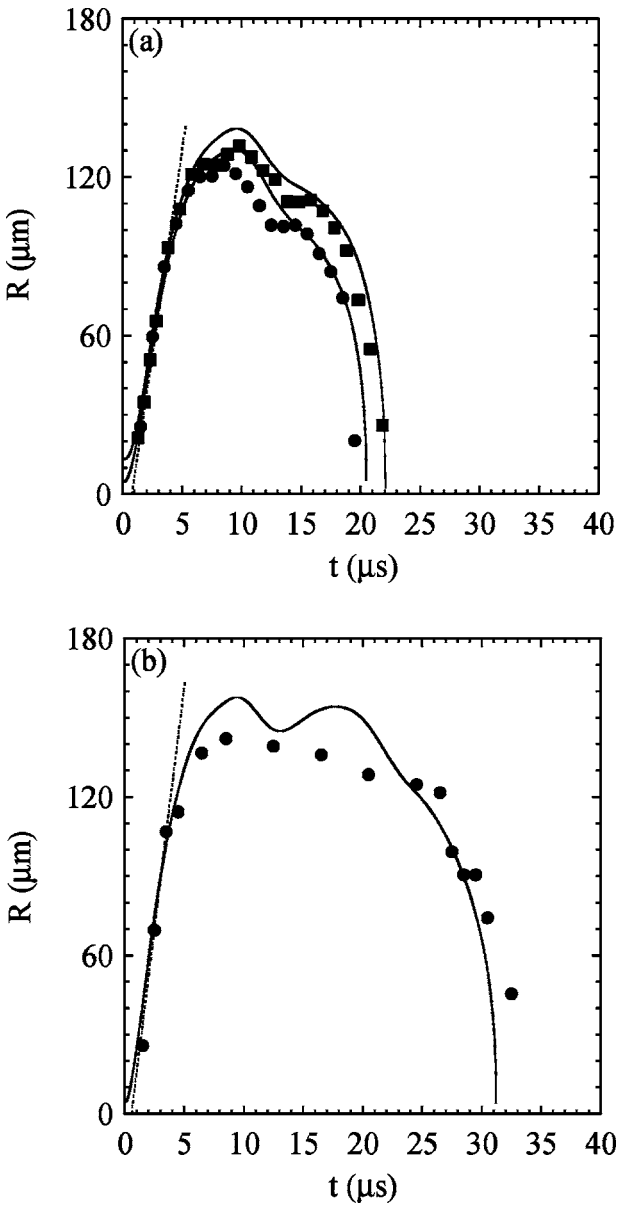

FIG. 3. (a) Time evolution of the bubble radius $R(t)$ for two initial cavity diameters D, (●) 4 μm and (■) 20 μm, subjected to a negative pressure of −1.4 MPa. The continuous curves represent the dynamics predicted by the Rayleigh-Plesset equation [(1)]. The slope of the straight dashed line is given by the estimate (3). (b) Same as in (a), but now for a negative pressure of −2 MPa. Note that the bubble gets more expanded than in (a) and the collapse takes longer.

adjusted in order to capture the overall trajectory of the bubble. This adjustment has been made for all the pressure levels using a cavity diameter of 4 μm. The relative amplitude correction is equal to a few percent and may arise from a bias of the optical fiber used for measuring the pressure as well as a possible mismatch between the spatial locations of the measurement and the cavitation experiment. In order to test the validity of this correction, we used two different cavity diameters, and thus two initial radii R_0, the first being used for the calibration. The corresponding theoretical evolution of $R(t)$ is compared with the experiments in Fig. 3(a), where we observe a good agreement for the two conditions. The good agreement validates the present approach, which

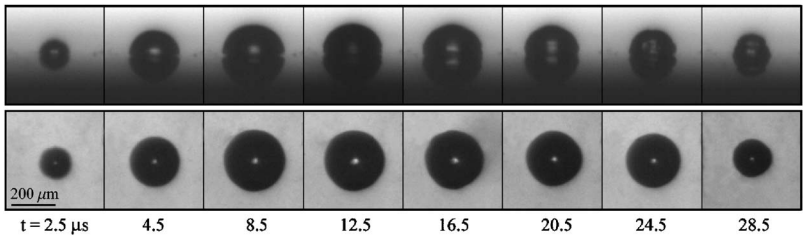

FIG. 4. Top and side views of the expansion and collapse of an isolated bubble subjected to a negative pressure of −2 MPa.

assumes an analogy between a free bubble and the hemispherical bubble growing on the substrate where the wall effect is negligible and acts only as a mirror. The comparison between experiment and theory for a higher forcing pressure is also reported in Fig. 3(b).

We note here that, for convenience, the high-pressure front has been removed for the integration since it does not play any role in the expansion phase. We also mention that for an even stronger forcing several bubbles emerge from one single microcavity and rapidly merge into one bigger bubble. This multinucleation event is due to the compression phase of the pressure wave which may destabilize the liquid/gas interface stretched on the cavity and therefore promotes many nuclei for cavitation. The real mechanism of this multibubbles formation remains to be understood.

The vorticity generated from the wall should affect a region near the wall on a thickness δ evolving with time like $(\nu t)^{1/2}$, where ν is the kinematic viscosity of the liquid. The overall cavitation event lasts less than 100 μs for all the experiments reported in this paper. Therefore, viscous effects are confined in a layer close to the wall less than 10 μm, which is small compared to the bubble size for almost all its lifetime.

The viscosity plays an important role in the motion of the contact line between the solid, the liquid, and the vapor. Indeed, due to viscous dissipation, the maximum speed of the contact line is only of the order of 1 cm/s (see, e.g., Quéré[30]) and it is therefore basically pinned close to the cavity. The substrate is not dried and a thin liquid film is formed between the bubble and the solid wall as observed in Fig. 4. An enlargement of a hemispherical bubble and the corresponding thin liquid film, which thickness should be correlated to δ, is shown in Bremond *et al.*[31]

IV. THE BUBBLE PAIR: WEAK INTERACTION

Since the cavitation of an isolated bubble is a rare event, we have designed some substrates dedicated to the study of the bubble pair interaction as a first step towards the multibubbles interaction. The control parameters are the distance d between the two hydrophobic cavities and the amplitude p_m of the negative pressure pulse. We first focus on the weak interaction regime where the maximum extension of each individual bubble is smaller than the initial separation d. An example is reported in Fig. 5 for a 400-μm pitch. As observed from the combined top and side views, the bubbles evolve as hemispherical caps during most of the lifetime of the doublet, except during the collapse phase where the bubbles tend to form jets towards each other and parallel to the wall. The time evolution of the bubble radius, which is the average of the two bubbles, is plotted in Fig. 6 for a distance d of 400 μm and two different acoustic pressures. For comparison, the dynamics of an isolated bubble is also shown for each case. The main feature of the interaction, which is more visible for the higher negative pressure, is the delay of the collapse. The relative delay between the isolated and the pair configurations is about 10% for a tensile strength of −1.4 MPa and 18% for for a tensile strength of −2.0 MPa.

If the two bubbles are not far from each other, the pressure induced by one bubble itself modifies the dynamics of the neighboring bubble and vice versa. Assuming that the pressure induced at a distance d from one bubble center is uniform around the surface of the second one and neglecting compressibility effects, the dynamics of the bubble radii, which are identical by symmetry, are described by a modified Rayleigh-Plesset equation (see, e.g., Pelekasis *et al.*[17]),

$$R\ddot{R} + \frac{3}{2}\dot{R}^2 = \frac{1}{\rho}\left(p_i(t) - p_l(t) - \rho\frac{R}{d}(R\ddot{R} + 2\dot{R}^2) - \frac{2\sigma}{R} - \frac{4\mu}{R}\dot{R}\right). \quad (4)$$

Equation (4) is numerically integrated by using the experimental pressure recording (Fig. 2). The resulting bubble radius $R(t)$ is plotted in Fig. 6 together with the experimental one. The coupling between the bubbles, corresponding to the terms proportional to $1/d$ in Eq. (4), is enough to capture the delay of the collapse and the overall dynamics is also fairly well described. It is surprising that this simple approach works so well since the maximal extension reaches nearly

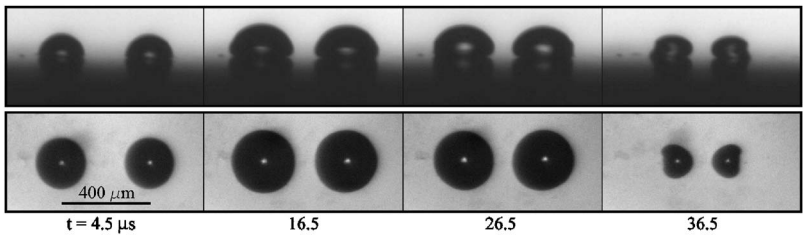

FIG. 5. Top and side views of the interaction of two bubbles initially at 400 μm apart from one another and subjected to a negative pressure of −2 MPa.

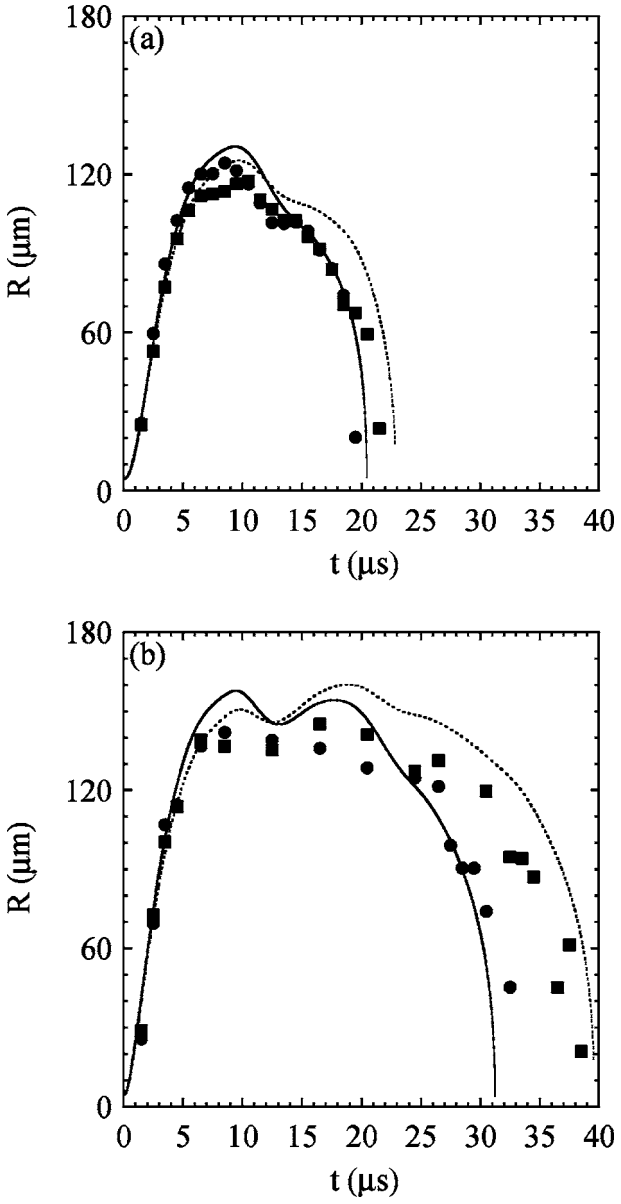

FIG. 6. (a) Time evolution of the bubble radius $R(t)$ (■) for two cavities at $d=400$ μm and subjected to a tensile stress of −1.4 MPa. The dashed line is the dynamics ruled by Eq. (4). The single-bubble case is also plotted (●), highlighting the delay of the collapse of the bubble pair. (b) Same as in (a), but now for $p_m=-2$ MPa.

75% of half of the initial distance d. The induced pressure is certainly not uniform around the bubble surface and induces a slight elongation of the bubbles as observed in Fig. 5 at $t=26.5$ μs. Nevertheless, this experiment confirms that this simple way of bubble coupling is meaningful and enough for describing the interaction of cavitation bubbles with slight shape deformation.

V. THE BUBBLE PAIR: STRONG INTERACTION

If the two cavities are initially closer to each other, or if the amplitude of the negative pressure peak is increased, the bubbles lose their spherical shape since the pressure induced by the twin bubble is not uniform anymore around the bubbles' surface. We call this regime the strong interaction regime. An example is shown in Fig. 7, both from the top and from the side. As the bubbles flatten when pushing against each other, a liquid film develops, which possibly ruptures, leading to bubble coalescence.

A. Film thinning

The time evolution of the gap h between the two bubbles measured along the line joining the two bubble centers is reported in Fig. 8 for three different collision conditions. The gap size decreases quickly with a speed comparable to the initial surface velocity U_0 of an isolated bubble given by Eq. (3). Therefore, the thinning rate is faster for higher amplitude of the negative pulse. The thinning then slows down to a velocity about ten times smaller. The accuracy of the measurement is limited by the spatial resolution of an individual picture where 1 pixel corresponds to 1.5 μm. As shown in Fig. 8, this limit is reached much sooner for smaller initial distance d between the two cavities.

The evolution of the film formed between the two bubbles is deduced from the analysis of Doubliez.[32] This analysis is valid for two bubbles in the bulk and will be applied here by assuming that the wall is a plane of symmetry and neglecting the boundary layer development on the wall as justified by the previous observations. The flow induced by the head-on collision of the two bubbles is axisymmetric, the line of symmetry being the axis z on the wall which joins the centers of the two bubbles as sketched in Fig. 9. We assume that the film thickness h is only a function of time t, and not of the radial position r. As the dynamic viscosity of the gas inside the bubble is two orders of magnitude less than the one of water at 20 °C, the bubble surface is considered as a shear free interface (i.e., fully mobile) and the effect of gas motion inside the bubble on the liquid is therefore neglected. As the water is assumed to be free of surfactant, the surface tension is constant and therefore there is no additional stress at the interface. Under these assumptions, the radial flow $u(r)$ is uniform through the liquid gap h, i.e., of a plug flow type. The condition of uniform film

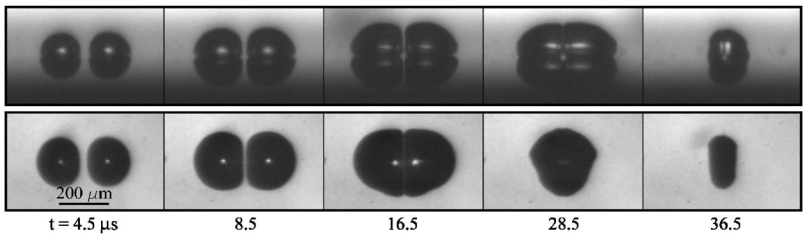

FIG. 7. Top and side views of the growing and flattening of two bubbles initially at $d=200$ μm and subjected to $p_m=-2$ MPa.

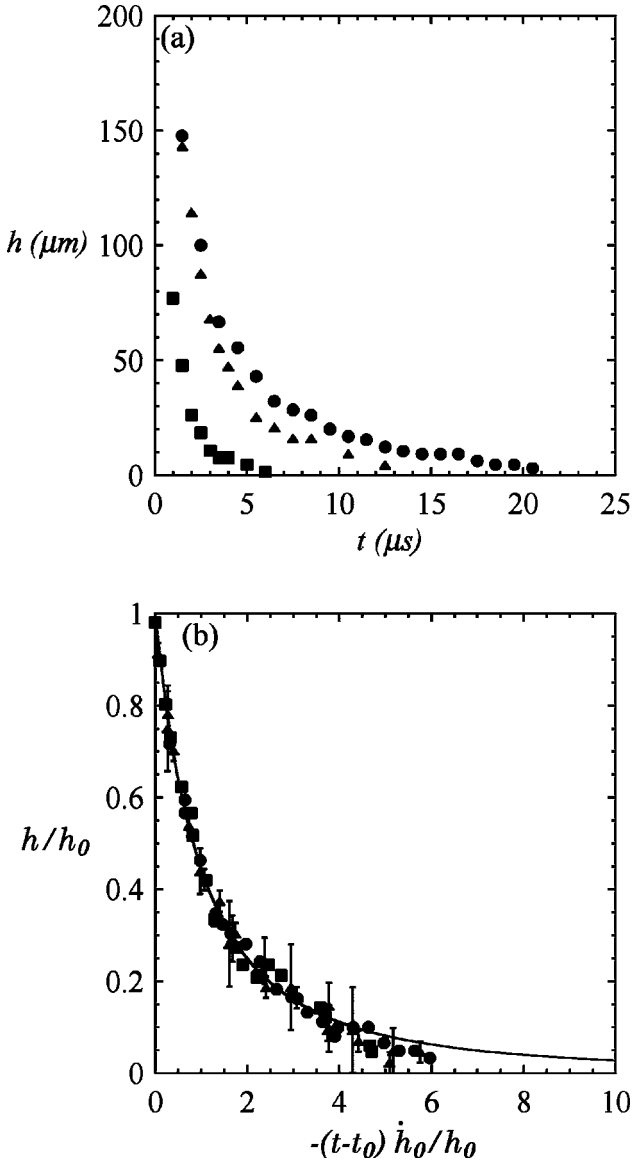

FIG. 8. (a) Time evolution of the film thickness h measured along the line joining the two bubble centers for several configurations: (●) $d=200$ μm and $p_m=-1.4$ MPa, (▲) $d=200$ μm and $p_m=-2.0$ MPa, (■) $d=100$ μm and $p_m=-2.0$ MPa. (b) Dimensionless film thinning for three pressure conditions: (●) −1.4 MPa, (■) −2.0 MPa, (▲) −2.9 MPa, and for d varying between 25 and 200 μm, compared with the inertia model given by Eq. (5) (continuous line).

thickness implies that the pressure in the film is independent of the radial position r; the film is bounded by two interfaces with a disk-like shape. The film drainage $h(t)$ is then a purely inertia-driven flow and is given by[32]

$$\frac{h(t)}{h_0}=\left(1-\frac{1}{2}\frac{\dot{h}_0}{h_0}(t-t_0)\right)^{-2}. \tag{5}$$

Here h_0 and $\dot{h}_0$ are, respectively, the initial thickness and the initial thinning velocity at $t=t_0$ when the two bubbles start to flatten and form a liquid film between them. $\dot{h}_0$ is equal to the approach velocity of the two bubbles at the onset of the flattening which can be estimated from the initial velocity U_0 of the bubble wall defined by Eq. (3),

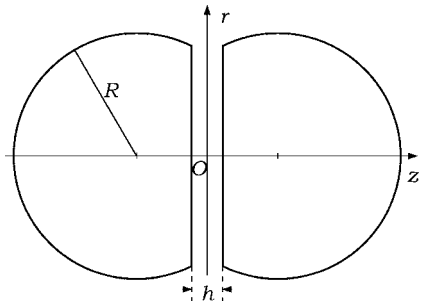

FIG. 9. Sketch of the film thinning between two bubbles.

$$\dot{h}_0=-U_0. \tag{6}$$

This estimate is valid if the onset time t_0 of the flattening falls in the interval where the bubble wall velocity U_0 is constant. The film thinning model describes an inertia process which thus depends on initial conditions h_0, U_0 at $t=t_0$. When the film is formed, a modification of one of them will just delay or postpone the time t_0. Moreover, a modification of U_0 by 10% leads to a decrease/increase of h_0 by 5%. That is why we have decided to set the same initial condition of the velocity U_0 with respect to the minimum pressure p_m and to fit the data with Eq. (5) by only tuning h_0. The values of h_0 and t_0 deduced from the experimental film thinning for different collision conditions are reported in Table I. The film formation time t_0 is always smaller than 3 μs and therefore falls in the initial phase of the expansion where the bubble wall trajectory is linear (Fig. 3). As expected, we note that the onset time t_0 of flattening decreases as the d decreases, but the evolution with the pressure forcing at a given interdistance d is not clear. We mention here that the value of t_0 is not absolute since the origin of time of the bubble dynamics in the experiments is not known *a priori*. The experimental origin of time is adjusted from the theoretical prediction of $R(t)$ when compared to a single bubble for each individual pressure level p_m. A comparison of t_0 for different pressure levels seems not to be relevant since they differ in a few tens of microseconds at constant pitch.

The experimental evolution of the film thickness h normalized by the initial thickness h_0 is plotted against the di-

TABLE I. Adjusted values of the onset time t_0 of the film formation and its initial thickness h_0 using Eq. (5) for several experimental configurations. The observed coalescence time t_c of the two bubbles is also reported.

p_m (MPa)	d (μm)	t_0 (μs)	h_0 (μm)	t_c (μs)
−2.9	200	2.9	66	⋯
	100	1.75	31	25
	50	1.4	16.5	14
−2.0	200	2.8	76	⋯
	100	1.8	32.5	30
	50	1.5	16.5	18
	25	0.5	13	10
−1.4	200	2.55	93	⋯
	50	1.6	19	18
	25	0.4	14	10

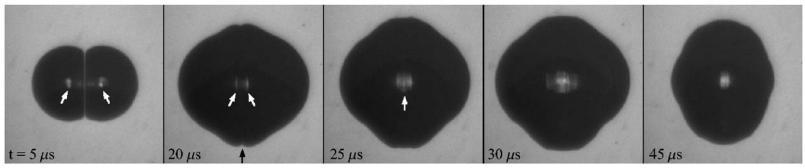

FIG. 10. Coalescence of two bubbles captured in the picture at the center ($t=25$ μs) for $d=100$ μm and $p_m=-2.9$ MPa. This event corresponds to the merging of the two light spots into one as indicated by the white arrows and the disappearance of the cusp pointed out by the black arrow.

mensionless time $-(t-t_0)\dot{h}_0/h_0$ in Fig. 8(b). Once the initial conditions of the film thinning are adjusted, all the experimental data fall on a master curve described by the purely inertial model given by Eq. (5). The error bars are estimated from the accuracy of the gap measurement, which corresponds to 1.5 μm.

B. Coalescence

A merging event is depicted in Fig. 10. The coalescence event is only caught by means of the evolution of the interface shape. Since the phenomenon is observed from above in reflection mode, only the light reflected by an area having a weak slope is captured by the camera. Two distinct bright spots, located at the top of each bubble, are visible in the first two frames and are pointed out by white arrows. The coalescence of the bubbles at $t=25$ μs is revealed by the merging of the bright spots. Another morphology change is the disappearance of the cusp located along the plane of symmetry and indicated by a black arrow in Fig. 10. Actually, this is not a real cusp since the bubbles are still separated by a thin liquid film. The interface is smoothed by the surface tension once the film breaks and therefore reveals the merging of the bubbles.

According to standard theory, the bursting of the film leading to coalescence is a thermally activated phenomenon:[33] the energy cost for the nucleation of a hole in the film is of the order of σh^2, with the energy of activation being a few kT, and thus the film bursts for thickness of the order of 1 nm. In contrast, critical film thicknesses prior to bursting are experimentally observed to lie between 10 and 100 nm (Ref. 34). The discrepancy of the critical thickness can be explained by the amplification of surface perturbations due to the destabilizing van der Waals attraction.[35,36]

In the present experiment, the lack of optical resolution does not allow us to resolve such small length scales. All that we can observe is that bubbles for initial bubble distance d smaller than 200 μm coalesce; the time of coalescence is reported in Table I. However, the present setup can be used for investigations of the effect of dissolved ions on the coalescence. Indeed, dissolved ions have been shown to either inhibit or enhance coalescence, depending on its type.[37]

VI. BOUNDARY INTEGRAL (BI) CALCULATIONS

The Rayleigh-Plesset analysis breaks down once the bubbles are too close and lose their hemispherical shape. However, the wall still acts as a mirror and is therefore still a plane of symmetry. In addition, the z-axial symmetry is conserved (where z is the line joining the centers of the bubbles, see Fig. 9). Taking advantage of the two symmetries of the system, we have used an axisymmetrical boundary integral code[38] in order to describe the overall shape evolution of the cavitating bubbles on the wall. The features of the numerical scheme are based on the method developed by Oğuz and Prosperetti.[39,40] The validity of the code has first been tested for the one-bubble case by comparing it to the solution of the Rayleigh-Plesset equation.

We then proceed with the two-bubble case. The contours of the two bubbles are compared with experimental top views in Fig. 11 for two different initial spacings d. The minimum pressure p_m is equal to -1.4 MPa in both cases. Each snapshot on a row corresponds to the time noted on the right-hand side of the figure. In both cases, the shape evolution of the bubble pair is well captured by the BI simulation. The overall size of the bubbles is slightly overestimated, an effect attributed to the viscous stress exerted on the bubble surfaces in the real situation.

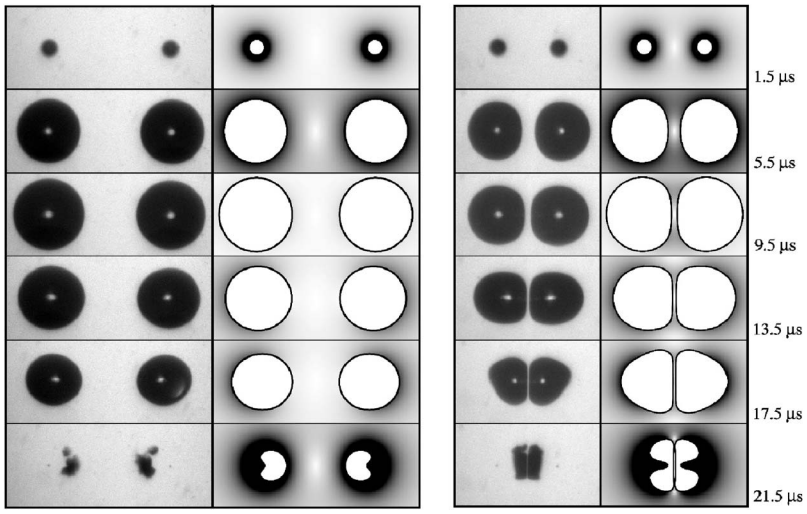

FIG. 11. Comparison between experiment and simulation of the cavitation of two bubbles initially set at a distance d equal to (left) 400 μm and (right) 200 μm subjected to a minimum pressure of -1.4 MPa. The time indicated on the right-hand side is the same for both sequences. The velocity field is superimposed with a grayscale where white corresponds to zero velocity and black to a velocity equal to or larger than 10 m/s.

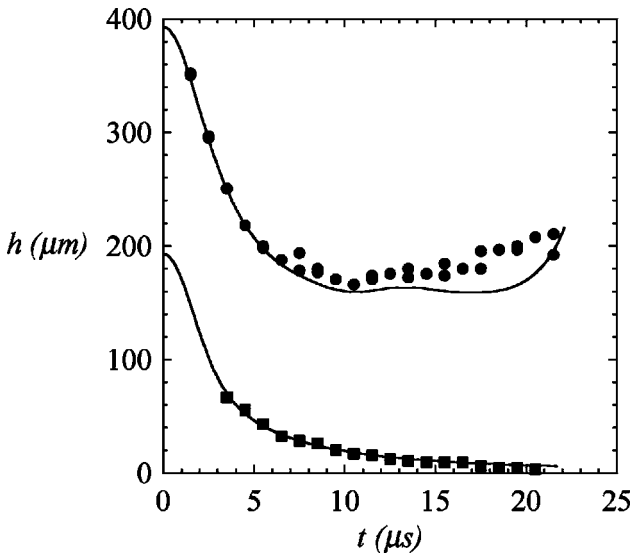

FIG. 12. Time evolution of the film thickness h between the bubbles for the same conditions as in Fig. 11 (p_m=−1.4 MPa, (●) d=400 μm, and (■) d=200 μm). The solid curves represent the thinning predicted by the BI simulations.

The BI simulations reveal the development of two *wall-parallel* jets at the final stage of the collapse. These jets are directed towards the center of the pair. *Wall-normal* jets are well known for the collapse of a bubble close to a solid boundary which breaks the spherical symmetry of the inner flow during the collapse:[11,41] one side of the bubble accelerates inward more rapidly than the opposite side leading to the formation of the reentrant jets. Here the symmetry breaking is due to the neighboring bubble and the jets are wall parallel.

To further compare the BI simulations with the experiments, the time evolution of the film thickness h squeezed between the bubbles is reported in Fig. 12. The good agreement between theory and experiment *a posteriori* justifies the potential flow approach used here for the description of cavitating hemispherical bubbles on a solid boundary which acts only as a mirror.

We have finally designed a substrate where five microcavities are aligned and spaced by 200 μm. The symmetry of this configuration being axial, we can use the present BI code for solving this multibubble case in a strong interaction regime. A time series of top views observed experimentally as well as the corresponding contours given by the numerical simulation are reported in Fig. 13. The main features of the cavitation event are again well reproduced by the potential flow theory. We note that the overall process lasts longer than the two-bubble case, and even more than the isolated bubble case, due to mutual screening of the bubbles.[7] The bubbles located on the edges reach a larger size and start to collapse sooner. As for the bubble pair, a reentrant jet develops from the sides during the collapse phase. This is not the case for the inner bubbles, which are confined between two neighbors. They collapse from the side exposed to the open medium in a way similar to the pinch off of a liquid thread.

The simulations provide, in addition, the velocity and pressure fields of such system, which are hardly accessible via experiments because of short time scales brought into play. The velocity field is obviously not valid close to the solid boundary but gives the spatial distribution of the velocity beyond the boundary layer, which could be used to estimate the stress exerted on the surface and therefore on solid or organic particles like cells adhering to the surface.[42] The velocity field is superimposed in Fig. 11 with a grayscale where white corresponds to zero velocity and black to a velocity equal to or larger than 10 m/s. The velocity cutoff equal to 10 m/s has been chosen for imaging the far field. The velocity close to the bubble surface is much larger than 10 m/s during the initial expansion phase and during

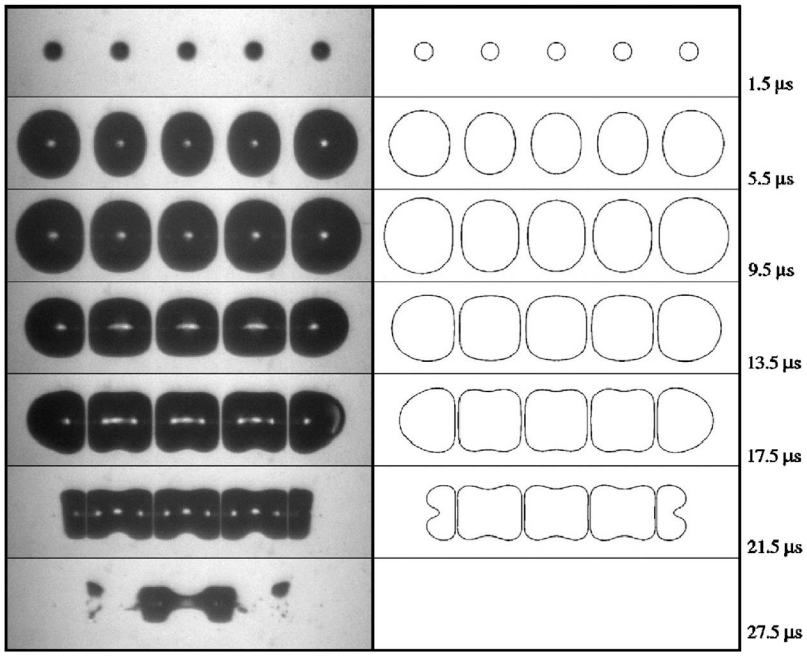

FIG. 13. Comparison between experiment and simulation of the cavitation of five bubbles set on a line with d=200 μm and p_m=−1.4 MPa.

the collapse where the reentrant jet can attain 70 m/s for $d=200$ μm and 90 m/s for $d=400$ μm.

VII. SUMMARY AND CONCLUSIONS

In this paper we have reported experimental and numerical results on the dynamics of cavitating bubbles on a solid surface and their interaction. We have developed an experimental procedure which allows one to control the spatial location of nucleation sites. The artificial nuclei are hydrophobic microcavities etched on a silicon plate. The microvoids trap air when the substrate is immersed in water and therefore promote cavitation of bubbles when the liquid pressure is lowered. The presence of the wall is found to act as a mirror, allowing a bulk approach for the description of the bubble dynamics. Indeed, an isolated bubble grows with a hemispherical shape with a radius well described by the Rayleigh-Plesset equation, which is normally only valid for spherical bubbles.

We have designed probes dedicated to the study of bubble pair interaction. Two regimes are considered here. The first one corresponds to weak coupling where the bubbles do not come into contact and keep a hemispherical shape for most of their lifetime, except during the collapse where they form a jet directed towards each other. The dynamics of the doublet is found to be well described once the pressure generated by each individual bubble is taken into account into the Rayleigh-Plesset equation. The collapse of the bubble pair is delayed due to mutual screening. Another regime is observed when the pressure forcing is increased or the initial distance between the cavities is decreased. Indeed, the bubbles flatten and form a thin liquid film between each other which can rupture, leading to coalescence. The film thinning is found to be driven by inertia of the liquid and therefore depends on the initial conditions of the film formation, the gap between the two bubbles, and the bubble surface velocity. The overall shape of the doublet is well captured by numerical simulations using a boundary integral method for both weak and strong interactions. The study has been extended to a line of bubbles where the evolution of the bubbles' size is a function of their spatial location.

From our study we conclude that despite the presence of the wall, the description of the dynamics of cavitation bubbles on a wall is well modeled by a potential flow analysis. The use of a boundary integral code is therefore valid and can be used for the evaluation of the pressure and velocity fields of such system.

ACKNOWLEDGMENTS

The authors acknowledge Claus-Dieter Ohl for valuable discussions and Han Garderniers and his collaborators for microfabrication support. Andrea Prosperetti and Mark Stijnman are gratefully acknowledged for developing the boundary integral code. This work is part of the research programme of the Stichting voor Fundamenteel Onderzoek der Materie (FOM), which is financially supported by the Nederlandse Organisatie voor Wetenschappelijk Onderzoek (NWO).

[1] J. C. Fisher, "The fracture of liquids," J. Appl. Phys. **19**, 1062 (1948).
[2] J. Frenkel, *Kinetic Theory of Liquids* (Dover, New York, 1955).
[3] S. Balibar and F. Caupin, "Metastable liquids," J. Phys.: Condens. Matter **15**, S75 (2003).
[4] Q. Zheng, D. J. Durben, G. H. Wolf, and C. A. Angell, "Liquids at large negative pressure: Water at the homogeneous nucleation limit," Science **254**, 829 (1991).
[5] C. E. Brennen, *Cavitation and Bubble Dynamics* (Oxford University Press, New York, 1995).
[6] N. Bremond, M. Arora, C. D. Ohl, and D. Lohse, "Cavitation on surfaces," J. Phys.: Condens. Matter **17**, S3603 (2005).
[7] N. Bremond, M. Arora, C. D. Ohl, and D. Lohse, "Controlled multibubble surface cavitation," Phys. Rev. Lett. **96**, 224501 (2006).
[8] L. Rayleigh, "On the pressure developed in a liquid during the collapse of a spherical cavity," Philos. Mag. **34**, 94 (1917).
[9] M. S. Plesset and A. Prosperetti, "Bubble dynamics and cavitation," Annu. Rev. Fluid Mech. **9**, 145 (1977).
[10] T. G. Leighton, *The Acoustic Bubble* (Academic, London, 1994).
[11] T. B. Benjamin and A. T. Ellis, "The collapse of cavitation bubbles and the pressure thereby produced against solid boundaries," Philos. Trans. R. Soc. London, Ser. A **260**, 221 (1966).
[12] A. Philipp and W. Lauterborn, "Cavitation erosion by single laser produced bubbles," J. Fluid Mech. **361**, 75 (1998).
[13] N. K. Bourne, "The collapse of cavities," Shock Waves **11**, 447 (2002).
[14] D. Krefting, R. Mettin, and W. Lauterborn, "High-speed observation of acoustic cavitation erosion in multibubble systems," Ultrason. Sonochem. **11**, 119 (2004).
[15] M. P. Brenner, S. Hilgenfeldt, and D. Lohse, "Single-bubble sonoluminescence," Rev. Mod. Phys. **74**, 425 (2002).
[16] E. A. Zabolotskaya, "Interaction of gas bubbles in a sound wave field," Sov. Phys. Acoust. **30**, 365 (1984).
[17] N. A. Pelekasis, A. Gaki, A. Doinikov, and J. A. Tsamopoulos, "Secondary Bjerknes forces between two bubbles and the phenomenon of acoustic streamers," J. Fluid Mech. **500**, 313 (2004).
[18] A. A. Doinikov, "Mathematical model for collective bubble dynamics in strong ultrasound fields," J. Acoust. Soc. Am. **116**, 821 (2004).
[19] G. Chahine and R. Duraiswami, "Dynamical interactions in a multibubble cloud," ASME J. Fluids Eng. **114**, 680 (1992).
[20] J. R. Blake, G. S. Keen, R. P. Tong, and M. Wilson, "Acoustic cavitation: the fluid dynamics of non-spherical bubbles," Philos. Trans. R. Soc. London, Ser. A **357**, 251 (1999).
[21] C. Wang and B. C. Khoo, "An indirect boundary element method for three-dimensional explosion bubbles," J. Comput. Phys. **194**, 451 (2004).
[22] Y. Matsumoto and S. Yoshizawa, "Behaviour of a bubble cluster in an ultrasound field," Int. J. Numer. Methods Fluids **47**, 591 (2005).
[23] Y. Tomita, A. Shima, and K. Sato, "Dynamic behavior of two-laser-induced bubble in water," Appl. Phys. Lett. **57**, 234 (1990).
[24] J. R. Blake, P. B. Robinson, A. Shima, and Y. Tomita, "Interaction of two cavitation bubbles with a rigid boundary," J. Fluid Mech. **255**, 707 (1993).
[25] J. P. Dear and J. E. Field, "A study of the collapse of an array of cavities," J. Fluid Mech. **190**, 409 (1988).
[26] B. Wolfrum, T. Kurz, R. Mettin, and W. Lauterborn, "Shock wave induced interaction of microbubbles and boundaries," Phys. Fluids **15**, 2916 (2003).
[27] J. Staudenraus and W. Eisenmenger, "Fiberoptic probe hydrophone for ultrasonic and shock-wave measurements in water," Ultrasonics **31**, 267 (1993).
[28] M. S. Plesset, "The dynamics of cavitation bubbles," J. Appl. Mech. **16**, 277 (1949).
[29] P. S. Epstein and M. S. Plesset, "On the stability of gas bubbles in liquid-gas solutions," J. Chem. Phys. **18**, 1505 (1950).
[30] D. Quéré, "Fluid coating on a fiber," Annu. Rev. Fluid Mech. **31**, 347 (1999).
[31] N. Bremond, M. Arora, C. D. Ohl, and D. Lohse, "Cavitation on patterned surfaces," Phys. Fluids **17**, 091111 (2005).
[32] L. Doubliez, "The drainage and rupture of a non-foaming liquid film formed upon bubble impact with a free surface," Int. J. Multiphase Flow **17**, 783 (1991).
[33] J. Bibette, F. L. Calderon, and P. Poulin, "Emulsion: Basic principles," Rep. Prog. Phys. **62**, 969 (1999).
[34] E. D. Manev and A. V. Nguyen, "Critical thickness of microscopic thin liquid films," Adv. Colloid Interface Sci. **114**, 133 (2005).
[35] A. Vrij and J. T. G. Overbeek, "Rupture of thin liquid films due to spon-

taneous fluctuations in thickness," J. Am. Chem. Soc. **90**, 3074 (1958).
[36]D. S. Valkovska, K. D. Danov, and I. B. Ivanov, "Stability of draining plane-parallel films containing surfactants," Adv. Colloid Interface Sci. **96**, 101 (2002).
[37]V. S. J. Craig, "Bubble coalescence and specific-ion effects," Curr. Opin. Colloid Interface Sci. **9**, 178 (2004).
[38]R. Bergmann, D. van der Meer, M. Stijnman, M. Sandtke, A. Prosperetti, and D. Lohse, "Giant bubble pinch-off," Phys. Rev. Lett. **96**, 154505 (2006).
[39]H. N. Oğuz and A. Prosperetti, "Bubble entrainment by the impact of drops on liquid surfaces," J. Fluid Mech. **219**, 143 (1990).
[40]H. N. Oğuz and A. Prosperetti, "Dynamics of bubble growth and detachment from a needle," J. Fluid Mech. **257**, 111 (1993).
[41]M. S. Plesset and R. B. Chapman, "Collapse of an initially spherical vapor cavity in the neighborhood of a solid boundary," J. Fluid Mech. **47**, 283 (1971).
[42]L. Junge, C. D. Ohl, B. Wolfrum, M. Arora, and R. Ikink, "Cell detachment method using shock-wave-induced cavitation," Ultrasound Med. Biol. **29**, 1769 (2003).